Temperature-dependent electrical, elastic and magnetic properties of sol–gel synthesized $Bi_{0.9}Ln_{0.1}FeO_3$ (Ln = Nd, Sm)

2012 J. Phys.: Condens. Matter 24 125901

(http://iopscience.iop.org/0953-8984/24/12/125901)

J. Phys.: Condens. Matter **24** (2012) 125901 (11pp) doi:10.1088/0953-8984/24/12/125901

Temperature-dependent electrical, elastic and magnetic properties of sol–gel synthesized $Bi_{0.9}Ln_{0.1}FeO_3$ (Ln = Nd, Sm)

J Schiemer[1,6], R L Withers[1], M A Carpenter[2], Y Liu[1], J L Wang[3,4], L Norén[1], Q Li[1] and W Hutchison[5]

[1] Research School of Chemistry, Australian National University, Acton, ACT, 0200, Australia
[2] Department of Earth Sciences, Cambridge University, Cambridge CB2 3EQ, UK
[3] Institute for Superconducting and Electronic Materials, University of Wollongong, Wollongong, NSW, 2500, Australia
[4] The Bragg Institute, ANSTO, Lucas Heights, NSW, 2234, Australia
[5] University of New South Wales at the Australian Defence Force Academy, Canberra, ACT, 2600, Australia

E-mail: schiemer@rsc.anu.edu.au

Received 17 August 2011, in final form 2 February 2012
Published 28 February 2012
Online at stacks.iop.org/JPhysCM/24/125901

Abstract
This report details correlated electrical, mechanical and magnetic behaviour in $BiFeO_3$ ceramics doped with 10% Ln (Ln = Sm, Nd) ions on the Bi, or perovskite A, site and synthesized by a sol–gel method. The ceramics exhibit bulk piezoelectric and ferroelectric properties and clear ferroelectric domain patterns through piezoresponse force microscopy. Resonant ultrasound spectroscopy, dielectric spectroscopy and magnetometry studies show correlated magnetoelectromechanical behaviour and the existence of weak ferromagnetism for both compositions. An anomaly with simultaneous mechanical and magnetic signatures is discovered in both materials near room temperature, while previously reported transitions and anomalies are found to exhibit electro- and/or magnetomechanical coupling. Magnetism is significantly enhanced in the Sm doped sample, which is a promising multiferroic material.

(Some figures may appear in colour only in the online journal)

1. Introduction

There has been rapidly growing interest over recent years in magnetoelectric multiferroics and on the associated interplay of their electrical, elastic and magnetic properties. Materials that exhibit such behaviour, particularly at room temperature and above, hold considerable promise for diverse applications including multi-state memory elements, spintronic devices as well as more conventional applications such as ferroelectric random access memory or piezoelectric devices.

The most promising single phase, multiferroic candidate material to date is $BiFeO_3$ (BFO), which is reported to exhibit essentially G-type antiferromagnetism (although this is complicated by an accompanying very long wavelength, ~62 nm, cycloidal spin modulation) as well as very strong ferroelectricity at room temperature and above [1]. BFO has a number of reported low temperature anomalies in behaviour, the existence and origin of which are contentious. These include a possible spin glass transition reported to occur in BFO near 30 K [2], with a possible spin glass to antiferromagnetic transition at ~250 K [3]. There are reports of frequency-dependent changes in the dielectric behaviour [4] and mechanical properties [5] of pure BFO around ~220 K, and there are possible anomalies in the magnetic properties at ~140 and ~200 K [6], or at least Raman spectra suggesting a magnetic anomaly. In the high

[6] Author to whom any correspondence should be addressed.

temperature region, BFO exhibits an antiferro–paramagnetic Neél temperature T_N of 640 K and a ferroelectric Curie temperature of 1100 K.

Unfortunately bulk BFO has been found to have an undesirably high leakage current, possibly due to its propensity to decompose into impurity phases at sintering temperatures [7]. Some powder processing methods, particularly leaching with nitric acid, have given powder that is pure to x-ray diffraction (XRD) sensitivity [8], but these powders are not as technologically useful as sintered ceramics. In addition, the cycloidal spin modulation is reported to preclude net magnetization and the observation of a linear magnetoelectric effect. On the other hand, experimentally the magnetization does exhibit a small jump at T_N, which is seemingly inconsistent with a regular antiferromagnetic transition [9].

Efforts to improve the intrinsic magnetic properties of pure BFO, in particular to induce a latent weak ferromagnetism, have focused largely on alkaline earth or rare earth/lanthanide substitution onto the Bi, or perovskite A site, position. Doping with isovalent rare earth (or lanthanide, Ln) ions, such as Ln = Nd^{III}, Sm^{III} or Gd^{III}, onto the Bi^{III}, or perovskite A site, of BFO has been effective in improving the magnetic and electromechanical properties over most pure BFO in thin film samples [10]. Weak ferromagnetism has been reported in studies on rare earth doped BFO [11], probably through interaction of the magnetic A site cations with the spin cycloid associated with the B site cations.

A recent study has shown that thin films of this $Bi_{1-x}Ln_xFeO_3$ type, when fabricated close to a rhombohedral ferroelectric to an orthorhombic antiferroelectric-like morphotropic phase boundary (MPB) region (around $x \sim 0.15$) [10], can have a comparable piezoresponse to the current most widely used $Pb(Zr_{1-x}Ti_x)O_3$, or PZT, piezoceramic material. Several $Bi_{1-x}Ln_xFeO_3$ (BLnFO) systems have also been investigated in bulk ceramic form [12], with reported piezoelectric coefficient, d_{33}, of up to 29 pC N^{-1} for both the Ln = Sm and Nd doped systems [13, 14]. Use of rare earth dopant has been shown to suppress secondary phase formation somewhat. BLnFO has more complicated high temperature behaviour, with a region of transformation from ferroelectric to antiferroelectric to paraelectric at approximately 400 K where Ln = Sm [10]. Low temperature behaviour has not been thoroughly investigated in rhombohedral BLnFO to date. Direct correlation between the various forms of order with temperature has also seen little investigation. In this rare earth doped $BiFeO_3$ study Sm is investigated, as it is the most promising candidate based on the aforementioned thin film work [10], and may lead to significant enhancements in both magnetic and electromechanical properties. Nd is used as a similar, but contrasting, element for the examination of properties, and to validate our synthesis method for other rare earth elements. From the literature, it is known that above ~10% of these rare earth dopants a transformation to an antiferroelectric-like state is expected [10, 12], while below 10% dopant, the temperature-dependent phase transition into the antiferroelectric-like state cannot be observed [10]. In order to examine room temperature ferroelectric domains and ferroelectricity-related properties, as well as to investigate the temperature-dependent transition into the antiferroelectric-like state, compositions with 10% Ln dopant on the A site have been used throughout this study.

With regard to synthesis approaches, there have been only a few reports of the use of the sol–gel approach for the synthesis of undoped BFO [15, 16], and none for the synthesis of BLnFO. In this study, we report the properties of rare earth doped BLnFO ceramics synthesized by a sol–gel route. This route gives rise to ceramic samples with improved purity and properties over most solid state synthesized samples, though with some leakage current and minor impurity phases still present. These samples are used to carefully investigate the temperature-dependent mechanical, magnetic and electrical properties, and the correlations between these, in an effort to throw further light on the complicated phase transitions reported in these systems. The techniques used to investigate correlated phase transition behaviour were resonant ultrasound spectroscopy (RUS), dielectric spectroscopy and magnetometry.

2. Experimental details

2.1. Synthesis

Initial work using solid state synthesis consisted of grinding together Bi_2O_3 (99%, Unilab), Nd_2O_3 (99.9%, Pi Kem) and Fe_2O_3 (99 %, Aldrich) followed by uniaxial pressing into 13 mm pellets and sintering at 870 °C for 2 h. This was found to give a comparable amount of impurity to other sintered pellet solid state samples in the literature [12].

$Bi_{0.9}Nd_{0.1}FeO_3$ (BNFO) and $Bi_{0.9}Sm_{0.1}FeO_3$ (BSFO) ceramics were synthesized via a low-aqueous, sol–gel process. For the $Bi_{0.9}Nd_{0.1}FeO_3$ (BNFO) sample, high purity (>98%) nitrate powders (neodymium nitrate hexahydrate (99.9%, Sigma), ferric nitrate nonahydrate (98%, Univar), bismuth nitrate pentahydrate (98.5%, Sigma) and anhydrous acetic acid (99%, Sigma)) were first dissolved in glacial acetic acid with stirring until a clear solution was obtained. The solvent was then slowly evaporated from this solution until a homogeneous gel was obtained. The gel was then dried at 180 °C for 24 h to remove all solvent, then ground in an agate mortar and pestle under ethanol and subsequently placed in an alumina crucible for heat treatment.

The powders were first placed under a heat lamp until spontaneous self-combustion began and then lidded and removed. These post-combustion powders were then heat treated for 2 h at 700 °C. They were then ground in a planetary ball mill consisting of yttria stabilized zirconia (YSZ) balls in polytetrafluoroethylene tanks under ethanol for 12 h. The milled powders were then mixed with PVA binder in an agate mortar and pestle and uniaxially pressed at 5 tonnes in a 13 mm steel die, before the binder was burnt out by heating at 600 °C for 2 h and sintering at 900 °C for 2 h. The final densities achieved were >95% of theoretical density. In order to validate the above sol–gel technique for rare earth ion doping in general, a 10% samarium doped bismuth ferrite ceramic sample was also synthesized, this time

using samarium nitrate hexahydrate (99.9%, Sigma), with the synthesis otherwise remaining the same.

2.2. Characterization

Conventional x-ray powder diffraction analysis was performed on a Siemens D5000 diffractometer. Further x-ray powder diffraction work was performed with a Guinier–Hägg camera using monochromatic Cu Kα1 radiation, with pure silicon (Sietronics GD#1) [17] added as an internal standard. The software package 'Unitcell' [18] was used for accurate determination of the resultant unit cell parameters.

In order to more carefully check for homogeneity as well as to establish the resultant compositions, the samples were qualitatively analysed via electron probe micro analysis (EPMA) using a JEOL 6400 scanning electron microscope (SEM) with an Oxford ISIS energy dispersive x-ray analysis (EDXA) detector (operating conditions: 15 kV, 1 nA, 39 mm working distance). Imaging was performed on a Hitachi 4300 SE/N field emission SEM (FESEM).

Domain imaging and switching observations were performed on a commercial scanning probe microscope (Cypher, Asylum Research) using an internal 15× high voltage amplifier and Olympus AC240TM electrilevers with spring constant $k \sim 2$ N m^{-1} and tip radius ∼25 nm. The dual frequency resonance enhanced approach (DART, Asylum Research) was used for domain imaging, with a contact force of approximately 100 nN. Piezoresponse curves were acquired from two loops using an AC signal ($f \sim 300$ kHz (resonant), $V_{AC} = 0.36$ V, phase offset = 180°) superimposed on a 0.2 Hz triangular square-stepping wave with bias up to ±60 V and a reading and writing time of 25 ms. The MicroAngelo nanolithography procedure (Asylum Research) was used for bitmap lithography experiments.

Resonant ultrasound spectroscopy (RUS) was performed for characterization of mechanical properties, internal friction, which influences mechanical quality factor, as well as to examine phase transitions and other temperature-dependent anomalies in elastic properties, in order to facilitate comparison with other measurement techniques. RUS was performed on parallelepiped samples cut from the 10% Nd doped and Sm ceramic pellets, with dimensions (2.238 mm × 3.231 mm × 1.124 mm) and (4.454 mm × 3.047 mm × 0.947 mm), respectively, using an annular diamond saw lubricated with paraffin. High temperature, low temperature and room temperature measurements were made on custom made equipment at the Department of Earth Sciences, Cambridge University, UK. RUS has previously been used to characterize many materials and minerals, including investigating phase transitions in materials similar in some ways to BFO, such as the tilted ferroelastic perovskite $SrZrO_3$ [19] and the magnetic perovskite $Pr_{0.48}Ca_{0.52}MnO_3$ [20]. Note that the peak frequencies measured by RUS are dependent on both the physical properties and the geometries of the samples used.

Low temperature RUS data were collected at temperatures from 5 to 300 K, using dynamic resonance system 'modulus II' electronics, and a standard orange helium flow cryostat, as described by McKnight *et al* [21]. Frequency was scanned from 100 to 1500 kHz with 50 000 data points per spectrum. High temperature data were collected from 300 to 750 K, in a frequency range of 100–1200 kHz, with 20 000 data points per spectrum, using alumina buffer rods protruding into a horizontal Netzsch furnace [22] and Stanford electronics described by Migliori and Maynard [23]. Internal friction, i.e. the inverse of quality factor Q, was obtained from asymmetric Lorentz fitting of the resonance peak, $Q^{-1} = \Delta f / f_0$. Δf is the full width at half maximum of the resonance peak, and f_0 is the resonance frequency of that peak. In order to examine trends in mechanical properties, f^2 values are commonly compared, as f^2 for predominantly shear modes of deformation is proportional to the shear modulus. Temperature measured by a thermocouple close to the sample was calibrated as described by McKnight *et al* [19].

Moduli were determined from fitting at least 24 peaks in room temperature spectra. A custom room temperature sample head was used, utilizing software also described by Migliori and Maynard [23], assuming that the ceramic samples were isotropic. DRS Modulus II electronics were used to generate the signal and process the output spectrum. The sample was mounted between two PZT-5A transducers, 2 mm in diameter, which were coated in gold to reduce radio interference.

In order to carry out electrical characterization, selected pellets were coated with silver paste on each side and then heat treated at 500 °C for 30 min to ensure good electrical contact. Dielectric properties were collected on a high precision LCR meter (Agilent 4284A), while ferroelectric hysteresis measurements were carried out on an aixACCT TF 2000 FE analyser. Piezoelectric properties were characterized on a Berlincourt type d_{33} meter (IACAS ZJ-6B, China).

Measurements of magnetization with temperature (M–T) were performed on a Quantum Design Magnetic Properties Measurement System (MPMS) superconducting quantum interference device (SQUID) magnetometer. M–T measurements were performed from 340 to 5 K in a 50 Oe magnetizing field (FC) after cooling the sample in zero field and warming up under 50 Oe field. M–H curves were acquired on a Quantum Design Physical Properties Measurement System (PPMS) vibrating sample magnetometer (VSM). M–H measurements were performed at 10, and 300 K, using up to 50 kOe field, on samples that had been cooled in 50 Oe field.

3. Results and discussion

3.1. Morphology and structure

3.1.1. Density, purity, cell dimensions and morphology. The use of sol–gel synthesis gave samples with excellent density (∼95–99%) when sintered at 900 °C for 2 h. The densities of the 10% Nd and Sm doped samples were 8.08 and 8.16 g cm^{-3}, respectively, as measured via the Archimedes method, equivalent to 98.2% and 98.9% of theoretical density as calculated using the unit cell parameters determined in this work. The pellets from which the samples cut for RUS

measurements were obtained were thicker and slightly less dense, at 94% and 95% of theoretical for the Nd and Sm doped samples, respectively. It is important to note that the density of RUS samples does not affect the temperature-dependent behaviour, and a correction can be applied to give the pore-free elastic moduli.

Sol–gel synthesis was found to improve phase purity by comparison with samples prepared via solid state reaction when examined by XRD. Conventional laboratory XRD was inconclusive, and for more accuracy these materials were examined with EPMA, with $<\sim 1\%$ of a $Bi_2Fe_4O_9$ impurity phase seen. These samples were further examined by the Guinier–Hägg XRD technique with a 1.5 h exposure (figure 1(a)(I)), and the intensity of the strongest impurity peak for $Bi_2Fe_4O_9$ is measured as $\sim 1.5\%$ of the strongest peaks of the major BLnFO phase and only slightly higher than the background intensity. A comparison of a sol–gel synthesized sample and the best solid state sample using scanned Guinier patterns is shown in figure 1(a)(II). This purity level is sufficiently high for analysis of property measurements and phase transition behaviour. These diffraction analysis results are comparable to the best obtained by using other techniques for synthesis of BLnFO samples [13, 14].

The samples were observed by XRD to be of rhombohedral (*R*3*c*) distorted perovskite phase. The unit cell volumes of the Sm and Nd doped samples were measurably different from one another and from a reference BFO unit cell. Both had contracted due to the smaller size of the dopant rare earth ion, with the contraction in the Sm doped sample greater, as expected. The rhombohedral unit cell of the 10% Nd doped sample in the hexagonal setting was 370.94 $Å^3$, with *a* and *c* parameters of 5.5713(3) Å and 13.7995(11) Å, while the unit cell volume of the 10% Sm doped sample was 370.50 $Å^3$, with *a* and *c* parameters of 5.5681(4) Å and 13.7988(12) Å respectively. By comparison, the unit cell volume of undoped $BiFeO_3$ [24] is 378.78 $Å^3$.

Microstructural investigation of pellet fracture surfaces with 10% Sm and 10% Nd by SEM shows a regular, well densified array of polyhedral grains with some intragranular pores (possibly due to some volatilization) (figure 1(b)). The grain size in the Sm doped ceramic is approximately 2.5 μm diameter (figure 1(b)(I)), while for the Nd doped ceramic the grain size is approximately 5 μm diameter (figure 1(b)(II)).

3.2. Room temperature behaviour

3.2.1. Electrical behaviour. For piezoelectric and ferroelectric measurements, the 10% Sm and Nd doped samples were polished to 160 μm thickness and 240 μm thickness, respectively. For piezoelectric measurements, they were poled using a, 150 kV cm^{-1} amplitude, triangular pulse in the ferroelectric analyser. The piezoelectric properties of these samples were then tested. BSFO 10 yielded a d_{33} of 18 pC N^{-1}, while BNFO 10 yielded a d_{33} of 22 pC N^{-1}, similar to previously reported results [13, 14]. Ferroelectric hysteresis loops could be obtained from both

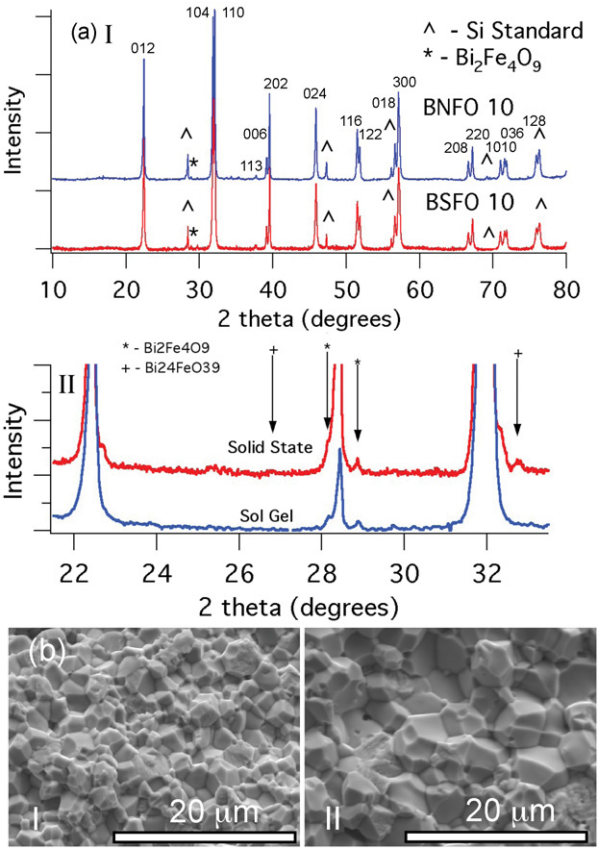

Figure 1. (a)(I) Guinier–Hägg XRD patterns, scanned from film and converted to intensity plots and (II) a comparison between the Guinier patterns for solid state and sol–gel synthesized samples of BNFO 10, scaled so that the strongest peak in each pattern is of equal intensity, and (b) SEM images of fracture surface morphology in (I) BSFO 10 and (II) BNFO 10.

samples (figures 2(a) and (b)), although some leakage current is present, as indicated by the rounding of the corners in their loops and by the coexistence of the polarization current (off-phase) and leakage current (in-phase, i.e. where the current and voltage are synchronous). BSFO 10 exhibits slightly higher leakage current relative to its polarization current when compared to BNFO (figure 2(c)). The coercive fields are 150 kV cm^{-1} for BSFO 10 (at 350 Hz) and 100 kV cm^{-1} for BNFO 10 (at 500 Hz), while the remnant polarization is ~ 20 μC cm^{-2} for both BNFO 10 and BSFO 10. Additionally, the dielectric breakdown strength of the materials limits the maximum applied field relative to the coercive field, particularly in BSFO, which makes direct comparison difficult and leads to the different position of the polarization current peaks (off-phase) in figure 2(c). The leakage current makes the polarization values less definitive, but clear ferroelectric switching is obvious. Electrical breakdown took place in both samples at slightly higher field than that shown, indicating the difficulty associated with switching the polarization of BFO-related ceramics. Dielectric measurements at room temperature (figure 3) show a relatively high loss at low frequencies, indicative of space charge motion, but at higher frequencies, this gives way to a low loss of 0.01 in BNFO 10 and 0.02 in BSFO 10 at

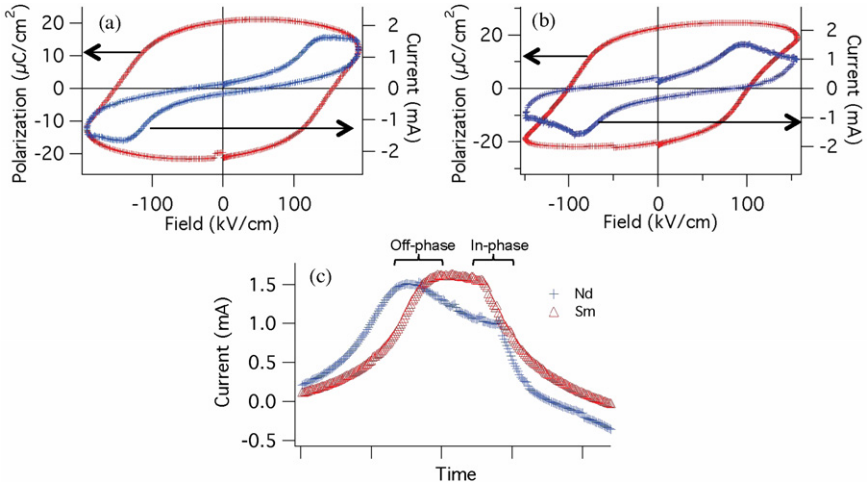

Figure 2. Ferroelectric hysteresis loops of (a) BSFO 10 (350 Hz) and (b) BNFO 10 (500 Hz), with current in blue and polarization in red, and (c) current traces versus time, normalized to frequency, with BNFO depicted with blue plus symbols and BSFO depicted with red triangles; current peaks are labelled by their phase relative to the applied voltage.

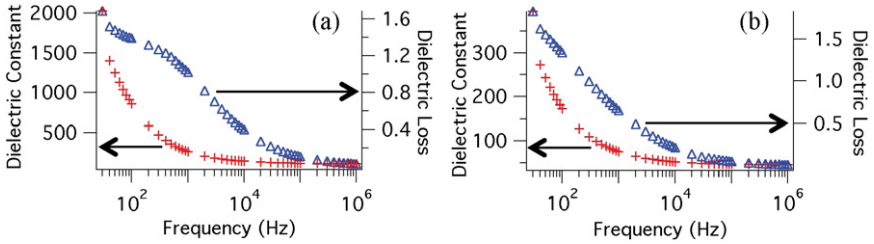

Figure 3. (a) Dielectric constant (red +) and loss (blue triangle) versus frequency for BSFO 10 at room temperature. (b) Dielectric constant (red +) and loss (blue triangle) versus frequency for BNFO 10 at room temperature.

1 MHz. There is some relaxation at low frequency in BSFO 10 (figure 3(a)).

Piezoresponse force microscopy (PFM) was carried out on 10% Nd and Sm samples polished to a thickness of ∼130 μm, followed by a final polish using 50 nm Al_2O_3 powder to achieve a good surface finish. All areas of both samples exhibited a strong piezoresponse and a rather regular ferroelectric micro-domain structure could be observed throughout (figure 4). Similar domain configurations were observed in both the BSFO and BNFO samples. Figure 4(a), for example, shows a 3 μm × 3 μm scan of the BSFO 10 and figure 4(b) an 8 μm×8 μm scan of the BNFO 10 sample. In both cases, larger domains can be seen into which needle-like ferroelectric domains have grown, reminiscent of what has been reported for rhombohedral PZT-related perovskites via electron microscopy [25]. At least three distinct domain orientations are apparent, as can be seen from the amplitude images (figures 4(a)(II), b(II)). The different amplitudes of these ferroelectric domains are probably due to their relative orientation with respect to the tip. It is possible that there is some weak contribution from electrostatic effects, but the clear 180° contrast in-phase shows which domains are predominantly in, and out, of the plane with respect to the tip and shows that piezoresponse is the dominant signal in these images. As these ceramics have grains of random orientation, and a resonance enhanced PFM technique with resonant peak tracking was used, no orientation has been assigned to the domains seen, nor any quantitative/pseudo-quantitative assignment of piezoresponse amplitude. A typical d_{zz} effective hysteresis loop for BSFO 10, obtained using a standard square-stepping triangular wave applied field, is shown in figure 4(a)(IV). Similar d_{zz} effective loops were also obtained for BNFO 10.

Polarization was also successfully performed on both samples to prove that they can indeed be poled and thus potentially be used for ferroelectric memory, or related, applications. A representative area in BNFO 10, for example, is shown in figure 5. The two small areas in figure 5 that do not appear to have poled properly (see the phase plot in figure 5(c)) are interpreted as having near in-plane components of ferroelectric polarization that could not be switched to become out of plane, as they still yielded piezoresponse loops when tested with switching spectroscopy. The difference in amplitude between up and down poled regions is probably due to electrostatic effects, as is common in PFM [26].

3.2.2. Mechanical behaviour. The measured, as well as porosity corrected, room temperature bulk and shear moduli of the 10% rare earth doped BFO samples were determined from the RUS spectra as described above and are given in table 1. These show that the BSFO 10 sample is significantly

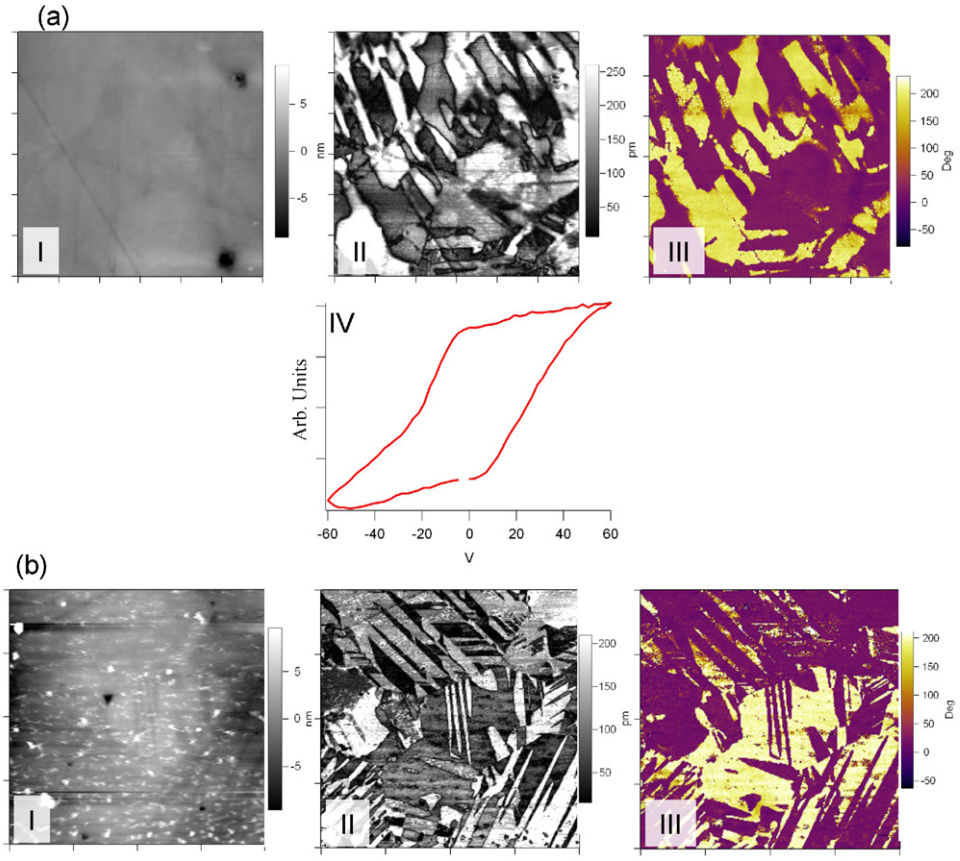

Figure 4. (a) Domain structures in BSFO 10 (3 μm $\times$ 3 μm scan) showing (I) morphology, (II) piezoresponse amplitude, (III) piezoresponse phase and (IV) a d_{zz} effective loop. (b) Domain structures in BNFO 10 (8 μm $\times$ 8 μm scan) showing (I) morphology, (II) piezoresponse amplitude and (III) piezoresponse phase.

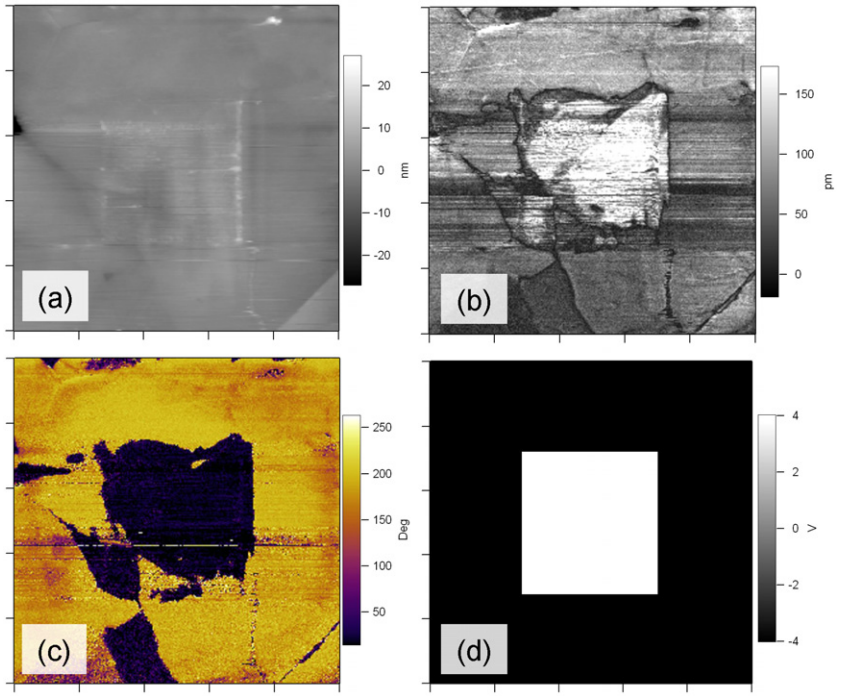

Figure 5. PFM imaging after square poling of an arbitrary region in BSFO 10 showing (a) morphology, (b) piezoresponse amplitude, (c) piezoresponse phase and (d) applied voltage. Clear phase and amplitude contrast shows successful poling in the region shown.

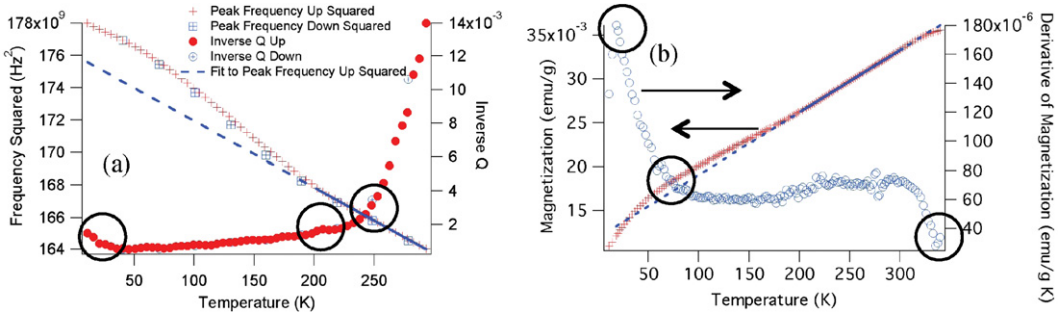

Figure 6. BSFO 10 low temperature data. (a) Processed low temperature RUS measurements on BSFO 10, with information from both increasing and decreasing temperature. A line is fitted to the 200–300 K data and shows excess stiffness below 200 K. (b) FC magnetic susceptibility versus temperature curve at 50 Oe and its derivative. The line shown is fitted to the 200–300 K data and shows an excess below the 200 K anomaly, a decrease below 60 K and a decrease above 300 K.

Table 1. Room temperature elastic properties of BNFO 10 and BSFO 10.

Sample	Bulk modulus (GPa)	Shear modulus (GPa)	RMS error (%)	Corrected bulk modulus (GPa)	Corrected shear modulus (GPa)	Density
BNFO 10	91.4	39.93	0.2976	105.0	45.1	7.702
BSFO 10	98.9	43.56	0.395	115.4	48.5	7.874
BFO (lit.)	97.3 [28]	—	—	—	—	—

stiffer than the BNFO 10 sample both in shear and bulk modulus, probably due to the smaller atomic size of the Sm^{III} ions. This provides an interesting parallel to the fact that BSFO is also electrically harder than BNFO, as discussed in section 3.2.1. The porosity corrected bulk and shear moduli were calculated using the relationships given in Ledbetter *et al* [27]. There has only been one previous report of the bulk modulus of pure BFO [28], given at the bottom of table 1. The relationship to the literature value of the bulk modulus for BFO given at the bottom of table 1 would be more reliable if taken with the same experimental method. Nonetheless, the measured bulk moduli of the BSFO 10 and BNFO 10 samples are close to and consistent with this previously reported value.

3.3. Low temperature behaviour

Given recent reports of anomalous low temperature behaviour in pure BFO [2, 4, 5, 9], temperature-dependent zero-field cooled magnetization and temperature-dependent analysis of particular peaks in the RUS data (to f^2 and Q^{-1}) were carried out to search for evidence of related anomalous temperature-dependent behaviour in the samples.

The BSFO 10 M–T curve (figure 6(b)) shows an overall increasing trend of susceptibility with temperature, which is expected for an antiferromagnet below its Neél temperature (T_N). There are, however, a number of anomalous regions in this plot, visible in the primary data but clearer in the derivative (circles in figure 6). Peak fitting to a prominent peak in the low temperature RUS spectra from BSFO 10 also reveals clear elastic anomalies (circled in figure 6(a)). There is a change in the derivative of the magnetization at 30 K from steeply increasing to steeply decreasing. This change in the magnetization below 30 K may be due to a paramagnetic/antiferromagnetic impurity such as $Bi_2Fe_4O_9$, as described by Lebeugle *et al* [1] (as a paramagnet displays $1/T$ susceptibility, even a tiny amount can give a relatively large signal as the temperature approaches zero), this temperature also corresponds with a small increase in Q^{-1} below ∼30 K in the BSFO 10 RUS and with a spin glass transition in BFO reported by Singh *et al* [2]. This 30 K magnetic anomaly is followed by a noticeable change in the derivative of magnetization at ∼70 K, followed by a relatively constant derivative up to about 190 K. The derivative changes again around 190 K, followed by a relatively constant derivative until about 300 K. The change at ∼190 K is at a similar temperature to the location of anomalies in found in magnetic data for undoped BFO [6]. There is also a much more prominent increase in mechanical Q^{-1} above ∼225 K, which is accompanied by a change in trend of the temperature-dependent behaviour of f^2 (proportional to the shear modulus). This appears to correlate with frequency-dependent changes observed in the dielectric behaviour [4] and mechanical properties [5] of pure BFO. Ramachandran and Rao [3] suggested that BFO has a spin glass to antiferromagnetic transition at ∼250 K and there is an anomaly in the magnetic properties at ∼200 K [6]. The combined change in f^2 and Q^{-1} observed here in RUS at ∼MHz frequencies resembles the pattern of elastic and anelastic behaviour associated with order/disorder processes in lawsonite [19] and Eu-doped $SrAl_2O_4$ [29]. With falling temperature, some dynamical disordering process couples with strain such that there is an acoustic loss, which diminishes as the stability field of the ordered phase is approached. The ordered phase displays little or no anelastic loss and an increase in stiffness, which is related to the order parameter. The increase in shear modulus associated with this

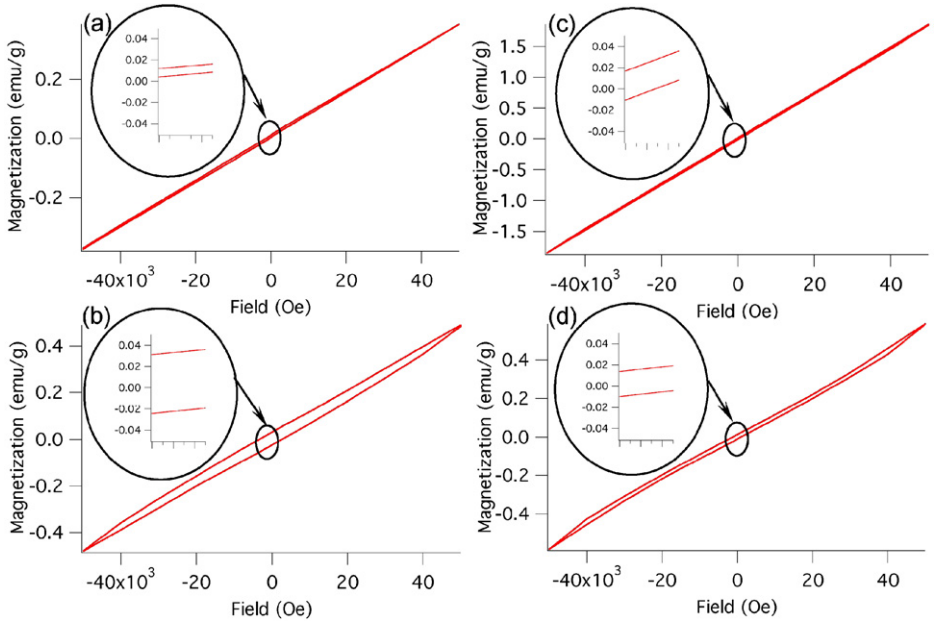

Figure 7. Magnetization versus field curves for BSFO 10 *M–H* at (a) 10 K and (b) 300 K and BNFO 10 (*M–H*) at (c) 10 K and (d) 300 K.

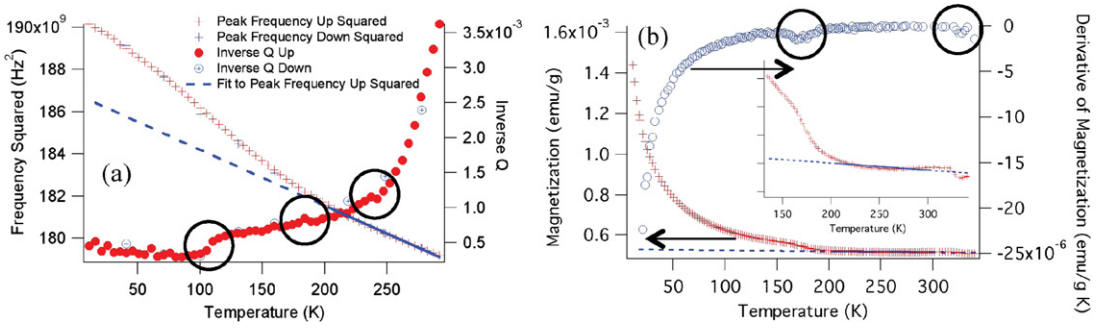

Figure 8. BNFO 10 low temperature data. (a) Analysis of low temperature RUS measurements, with information from both increasing and decreasing temperature. A line is fitted to the 200–300 K data and shows excess stiffness below 200 K. (b) FC magnetic susceptibility versus temperature curve at 50 Oe and its derivative. The inset shows a linear fit to the 200–300 K data, showing excess magnetization from the anomaly at ∼190 K.

ordering is given by the difference between observed values and extrapolation of a linear fit to the data from 200 to 300 K in figure 6(a). Similarly, if a straight line is fitted to the *M–T* data from 200 to 300 K and extrapolated beyond the region of the 190 K magnetic anomaly (see figure 6(b)), an excess magnetization is found below the ∼200 K transition point in a similar way to the excess stiffness found via the same approach in the RUS data. Finally, there is a change in the derivative of magnetization above 300 K followed by a minimum at 340 K. The dip in derivative at 340 K is the onset of a temperature interval where the absence of resonance peaks in the RUS spectra signifies strong acoustic dissipation, as discussed in section 3.4. This may be connected with the transformation from the ferroelectric to the antiferroelectric state, which occurs just above this temperature in thin film samples [10].

BSFO 10 *M–H* curves show very weak ferromagnetism at 10 K (figure 7(a)), with a remnant magnetization of 0.003 94 emu g^{-1}, this is very small and may indicate that BSFO is, in fact, a pure antiferromagnet at 10 K. At room temperature, the remnant magnetization increases significantly, to 0.0277 emu g^{-1} (300 K) (figure 7(b)). The existence of remnant magnetization indicates that BSFO 10 is weakly ferromagnetic at room temperature and possibly at low temperature, although the disappearance of the magnetization may be expected if spin glass behaviour does occur at low temperatures.

The RUS behaviour of BNFO 10 in the low temperature range (figure 8(a)) is very similar to that of BSFO 10, although there is an additional anomaly in Q^{-1} at 110 K, which is at a similar temperature to the onset of a frequency change previously reported in Raman spectra [6]. The BNFO 10 *M–T* curve (figure 8(b)) shows a clear anomaly beginning near 165 K and ending at around 200 K (see the inset in figure 8(b)), as well as a significant increase in low temperature magnetization and another anomaly from 330 to 350 K. Again the 200 K anomaly shows excess magnetization below the transition point, as visualized by extrapolating

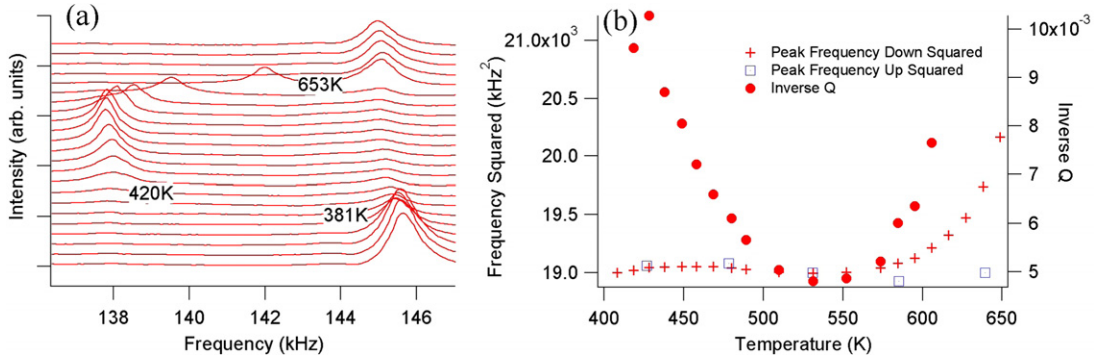

Figure 9. BSFO 10 high temperature data. (a) Peak trends with temperature for the first available resonance at elevated temperature, showing a strong dissipation effect at around 400 K, with associated softening, and a significant stiffening at around 650 K. (b) Processed data for the peak shown in (a), showing peak frequency and inverse quality factor. Two anomalies are clearly visible, with associated peaks in the dissipation. Some hysteresis is seen around 640 K, with a difference between peak frequencies up and down of the order of 4 kHz.

a linear fit to the data from 200 to 300 K. The reason for the greater relative magnitude of the low temperature paramagnetic increase in magnetization in the BNFO 10 sample than the BSFO 10 sample is likely to simply be because the response of the BSFO 10 sample at 50 Oe applied field is approximately an order of magnitude higher than that in BNFO 10, while the impurity levels, based on a careful examination of the XRD patterns, are similar. This is also likely to be obscuring any small anomalies in the magnetization in the BNFO 10 sample below 160 K, as well as the general upward trend in magnetization with temperature expected for an antiferromagnet below T_N. The 160–200 K anomaly is obvious as a dip in the derivative (figure 8(b)) and coincides with the 200 K anomaly found in the RUS measurements. One possibility, examined by a number of authors, is that the 160–200 K transition could be interpreted as being similar to the spin-reorientation transitions seen in orthoferrites [30]. While this interpretation has been shown to be incorrect in undoped $BiFeO_3$, the doping of magnetic rare earth ions onto the perovskite A site makes the materials in this investigation more closely related to the orthoferrites. Indeed, slightly more doping with rare earth ions or a slightly higher temperature makes these solid solutions assume the orthorhombic, orthoferrite structure rather than the rhombohedral $BiFeO_3$ structure [13]. Spin reorientations in orthoferrites involve two second-order transitions, with a period of reorientation between them, which the 40 K wide anomaly may correspond to. If the anomaly is not due to spin reorientation, as shown for undoped $BiFeO_3$, no solid explanation exists in the literature, but this examination of the magnetomechanical coupling may assist in finding one. The change in derivative appears to be qualitatively similar to that in the orthoferrites, but quantitative matching of theory to experimental results requires single crystal magnetization measurements that we do not have [31]. The anomaly from 330 to 350 K is at a very similar location to that in BSFO 10, and thus their origin is likely to be similar, again possibly due to the ferroelectric–antiferroelectric transition that occurs slightly above this temperature in BSFO 10 thin film samples [10].

The *M–H* behaviour of BNFO 10 is qualitatively similar to that of BSFO 10, but the magnitude of remnant magnetization is significantly smaller, indicating less ferromagnetic character. The *M–H* curves for BNFO 10 show weak ferromagnetism at 10 K (figure 7(c)), with a remnant magnetization of 0.0137 emu g^{-1}. At room temperature, the remnant magnetization remains relatively unchanged, at 0.0117 emu g^{-1} (300 K) (figure 7(d)). The existence of remnant magnetization at all temperatures indicates that BNFO 10 is weakly ferromagnetic throughout the temperature range investigated, but the remnant magnetization at room temperature is less than half of that for BSFO 10.

3.4. High temperature behaviour

Anomalies are apparent at high temperature in RUS measurements from both materials (figures 9 and 10). Resonance peaks from the sample alone are essentially absent from spectra collected between ∼380 and 420 K for BSFO 10 and ∼340 and 429 K for BNFO 10 (figures 9(a), 10(a)), though weak interactions between sample resonances and peaks from the alumina rods are still visible, rod resonance peaks are identified by being relatively temperature independent, as shown in figure 10(a). A high mechanical quality factor does not return until approximately 500 K, as can be observed in figures 9(a) and 10(a). It seems likely that this region of dissipation and change in frequency relates to a temperature-induced ferroelectric to antiferroelectric to paraelectric phase transition sequence reported in rare earth doped $BiFeO_3$ thin films, which occurs is the region of 400 K in a 10% Sm doped sample [10].

There is a decrease in the mechanical Q^{-1} with increasing temperature up to 520 K (figure 9(b)) in BSFO 10, which appears to be the high temperature side of a Debye-like dissipation peak for which the low temperature limit is ∼225 K, as discussed in section 3.3. Above ∼550 K, there is then an increase in Q^{-1} which is accompanied by an increase in elastic stiffness, which ceases to increase at 670 K, which is approximately the expected Neél temperature for this material.

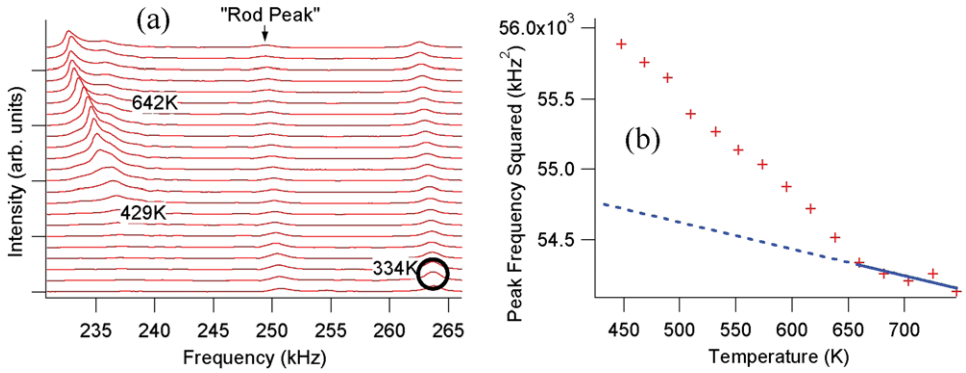

Figure 10. BNFO 10 high temperature data. (a) Peak trends with temperature for the first available resonance at elevated temperature, showing a strong dissipation effect at around 400 K, with associated softening, and a small stiffening at around 650–700 K. (b) Processed data for the peak shown in (a); a line is shown for reference, which is fitted to the 650–750 K data. This line shows a stiffening below 650 K, which is likely to be associated with an order–disorder process. Peak frequencies could not be estimated below or on the dissipative anomaly at around 400 K due to the high peak halfwidth and interaction with resonating alumina rod peaks, but a peak appears to be present in the circled area at ∼330 K, as determined from an anomalously high intensity in the rod peak at 264 kHz. The stiffening at 640 K appears to be preceded by a slight softening at 610 K.

RUS data using f^2 of a peak in the spectra from BNFO 10 also appear to have an increase in elastic stiffness below ∼650–700 K which corresponds closely to the Neél temperature for this material [32]. This is clearly shown by the extrapolation of a linear fit to the data from 650 to 750 K (figure 10(b)).

It has been reported elsewhere that 10% Sm doped $BiFeO_3$is a weak ferromagnet [11], while 10% Nd doped $BiFeO_3$ is an antiferromagnet [14]. Our own magnetometry data (section 3.3) suggest that the ferromagnetic component of behaviour in the Sm doped sample is significantly larger than that in the Nd doped sample. With this in mind, the qualitative difference between the RUS transition behaviours of Neél temperature in BSFO 10 and BNFO 10 may be partially due to their different magnetic ordering, with a larger effect seen in the more ferromagnetically ordered material.

4. Conclusions

Remnant magnetization at all temperatures in BSFO 10 and BNFO 10 indicates that these materials are true ferroelectric ferromagnets at room temperature. RUS and magnetometry anomalies were observed at very similar temperatures at low temperature, with excess elastic stiffness and magnetization observed below ∼200 K in both cases as well as observation of the proposed spin glass transition at 30 K. The RUS and magnetic data showed a similar anomaly at ∼350 K in both materials, with a large associated increase in mechanical dissipation, which may be associated with the onset of phase transitions into an antiferroelectric region, as reported in the literature. Near the Neél temperature in both materials, elastic anomalies were observed, again showing magnetomechanical coupling near this transition, which couples with previous reports of electrical anomalies in this region. Further investigation of the magnetic enhancement in these rare earth doped BFO systems is warranted, as considerable differences exist between the transition behaviours in the Ln = Nd and Sm systems.

Acknowledgments

The ANU Centre for Advanced Microscopy is thanked for provision of equipment and technical assistance. RLW, MC and YL appreciate the support of the Australian Research Council (ARC) in the form of a Discovery Grant. The RUS facilities in Cambridge were established through a grant to MAC from the Natural Environment Research Council (NE/B505738/1). YL also appreciates support from the ARC Future Fellowships programme.

References

[1] Lebeugle D, Colson D, Forget A, Viret M, Bonville P, Marucco J F and Fusil S 2007 *Phys. Rev.* B **76** 024116
[2] Singh M K, Prellier W, Singh M P, Katiyar R S and Scott J F 2008 *Phys. Rev.* B **77** 144403
[3] Ramachandran B and Ramachandra Rao M S 2009 *Appl. Phys. Lett.* **95** 142505
[4] Kamba S, Nuzhnyy D, Savinov M, Šebek J, Petzelt J, Prokleška J, Haumont R and Kreisel J 2007 *Phys. Rev.* B **75** 024403
[5] Redfern S A T, Wang C, Hong J W, Catalan G and Scott J F 2008 *J. Phys.: Condens. Matter* **20** 452205
[6] Singh M K, Katiyar R S and Scott J F 2008 *J. Phys.: Condens. Matter* **20** 252203
[7] Selbach S M, Einarsrud M A and Grande T 2009 *Chem. Mater.* **21** 169–73
[8] Arnold D C, Knight K S, Morrison F D and Lightfoot P 2009 *Phys. Rev. Lett.* **102** 027602
[9] Ramazanoglu M, Ratcliff W II, Choi Y J, Lee S, Cheong S-W and Kiryukhin V 2011 *Phys. Rev.* B **83** 174434
[10] Kan D, Pálová L, Anbusathaiah V, Cheng C J, Fujino S, Nagarajan V, Rabe K M and Takeuchi I 2010 *Adv. Funct. Mater.* **20** 1108–15
[11] Khomchenko V A, Paix J A, Shvartsman V V, Borisov P, Kleemann W, Karpinsky D V and Kholkin A L 2010 *Scr. Mater.* **62** 238–41
[12] Karimi S, Reaney I, Han Y, Pokorny J and Sterianou I 2009 *J. Mater. Sci.* **44** 5102–12
[13] Yuan G L and Or S W 2006 *J. Appl. Phys.* **100** 024109
[14] Yuan G L and Or S W 2006 *Appl. Phys. Lett.* **88** 062905

[15] Chen F, Zhang Q F, Li J H, Qi Y J, Lu C J, Chen X B, Ren X M and Zhao Y 2006 *Appl. Phys, Lett.* **89** 092910
[16] Nakamura Y, Yun K-Y, Nakashima S and Okuyama M 2007 *Integr. Ferroelectr.* **95** 226–33
[17] Sietronics Pty Ltd, ACT 2612, Australia
[18] Noläng B, Unitcell, S-74022 Bälinge, Sweden
[19] McKnight R E A, Howard C J and Carpenter M A 2009 *J. Phys.: Condens. Matter* **21** 015901
[20] Carpenter M A, Howard C J, McKnight R E A, Migliori A, Betts J B and Fanelli V R 2010 *Phys. Rev.* B **82** 134123
[21] McKnight R E A, Carpenter M A, Darling T W, Buckley A and Taylor P A 2007 *Am. Mineral.* **92** 1665–72
[22] McKnight R E A, Moxon T, Buckley A, Taylor P A, Darling T W and Carpenter M A 2008 *J. Phys.: Condens. Matter* **20** 075229
[23] Migliori A and Maynard J D 2005 *Rev. Sci. Instrum.* **76** 121301
[24] Pandey D and Singh A 2009 *Bull. Mater. Sci.* **32** 361–7
[25] Randall C A, Barber D J and Whatmore R W 1987 *J. Mater. Sci.* **22** 925–31
[26] Alexe M and Gruverman A 2004 *Nanoscale Characterisation of Ferroelectric Materials: Scanning Probe Microscopy Approach* (Heidelberg: Springer)
[27] Ledbetter H, Lei M, Hermann A and Sheng Z 1994 *Physica* C **225** 397–403
[28] Zhu J L, Feng S M, Wang L J, Jin C Q, Wang X H, Li L T, Li Y C, Li X D and Liu J 2010 *High Pressure Res.* **30** 265–72
[29] Carpenter M A, Howard C J, Andrew M J, McKnight R E A, Liu Y and Withers R L 2010 *J. Appl. Phys.* **107** 013505
[30] Sosnowska I, Steichele E and Hewat A 1986 *Physica* B+C **136** 394–6
[31] Bazaliy Y B, Tsymbal L T, Kakazei G N and Wigen P E 2004 *J. Appl. Phys.* **95** 6622–4
[32] Levin I, Karimi S, Provenzano V, Dennis C L, Wu H, Comyn T P, Stevenson T J, Smith R I and Reaney I M 2010 *Phys. Rev.* B **81** 020103